CHAPTER 155

CONTROL OF WAVE PROPAGATION ANGLE BY TAPERED-SUBMERGED BREAKWATER

Satoshi TAKEWAKA[1] and Isao IRIE[2]

ABSTRACT

A new type of submerged breakwater with a triangular plane form which modifies the wave propagation angle is proposed. Its performance is demonstrated and assessed analytically. Preliminary movable bed experiments were conducted. The breakwater was installed in front of the beach to modify the wave propagation angle in the offshore zone. Longshore current and littoral drift were driven through the effect of wave angle modification.

INTRODUCTION

A beach remains stable in the long term when supply and loss of sediment are equally balanced. Offshore structures often break this equilibrium state and the beach profile as well as the shoreline configuration change to a new state, which resulting in erosion problems in most cases. The deformation of the shore may be suppressed when sediment movement of the original state is preserved by regulating the wave height and propagation angle by some offshore structures.

In this context, a new type of submerged breakwater with triangular planeform, Tapered-Submerged Breakwater (hereafter referred as TSB), is proposed. Its functions are reduction of wave height by reflection and wave breaking, and modification of wave propagation angle on downwave side as shown in Fig. 1.

This study describes and evaluates the performance of TSB in controlling wave propagation angle. Then results of preliminary movable bed experiments are demonstrated , which were conducted to test out the applicability of TSB in regulating wave field, current system and sediment transport of a beach.

[1]Research Associate, Dept. of Civil Eng., Kyushu University, Fukuoka, Japan 812–81. Email : takewaka@civil.kyushu-u.ac.jp

[2]Professor, ditto, Email : irie@civil.kyushu-u.ac.jp

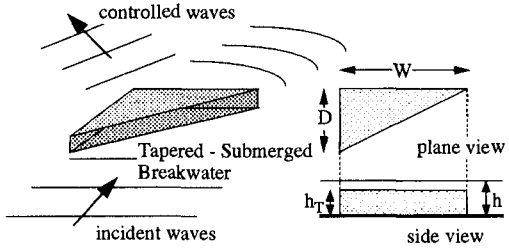

Figure 1 The concept of Tapered-Submerged Breakwater

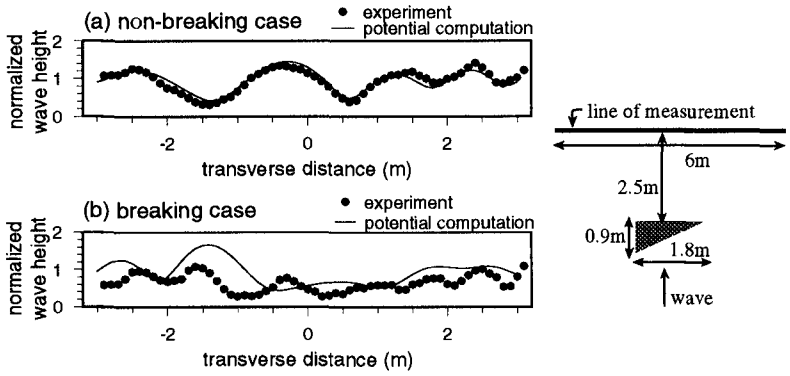

Figure 2 Normalized wave height distribution on downwave side of the breakwater. Wave height is normalized with the incident wave height. Experimental conditions : $T = 0.76s$, $h = 0.14m$, incident wave height $= 0.015m$, $W = 1.8m$, $D = 0.9m$, (a) $h_T = 0.07m$, $h_T/h = 0.5$, (b) $h_T = 0.11m$, $h_T/h = 0.8$.

MODIFICATION OF WAVE PROPAGATION ANGLE

The shape of a TSB is characterized with three parameters, height of breakwater h_T, plane depth D and plane width W, as shown in Fig. 1. All these parameters were varied in a wide range in this study to find out an optimum configuration of TSB in wave angle modification.

Wave field around TSB subjected to regular incident waves was computed with *Collocation Method of Matched Eigenfunction Expansions* which was developed by Yoshida et al.(1992). This method provides linear potential solution of wave field over a submerged structure with an arbitrary plane form. Prior to the analytical work, experiments in a wave tank were made to examine the validity of the potential solutions. Figure 2(a) and (b) show the comparison of measured and computed wave height distribution normalized with the incident wave height on the downwave side of the TSB.

A fairly good agreement is observed in Fig. 2(a), while discrepancy becomes

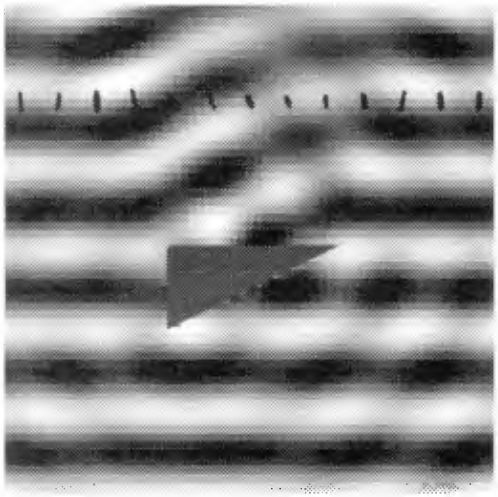

Figure 3 Wave pattern and trajectories of water particles. $T = 0.76s$, $h = 0.14m$, $W = 1.8m$, $D = 0.9m$, $h_T = 0.11m$, incident wave height $= 0.01m$. Incident wave travels from bottom to top in the figure.

apparent in Fig. 2(b) where wave breaking above the TSB was observed in the experiment. Since the potential solution fails to describe the wave field when wave breaking occurs, this study concentrates on non-breaking cases.

The wave height distribution shown in Fig. 2(a) oscillates remarkably which is a typical feature of wave diffraction from submerged a structure. Since the plane form of the submerged body is asymmetric in this study, the most energetic part appears aside from the center of the wave height distribution. This is an indication that the TSB modifies the direction of wave energy propagation.

The distribution of instantaneous water surface elevation and the horizontal trajectories of the water particle motion around the TSB is shown in Fig. 3. The incident wave travels from bottom to top of the figure. The water surface are shaded in this figure with the highest levels being white and trajectories of water particles are depicted with solid lines. Declined crest lines are apparent on the downwave side of the TSB. The main semiaxes of the water particle trajectory are almost perpendicular to the crest line which assures that the waves travel obliquely to the incident.

EVALUATION OF THE WAVE ANGLE CONTROL PERFORMANCE

The performance of the wave propagation angle modification is assessed by analyzing the character of the potential solution provided from the Collocation Method. The Collocation Method gives the complex amplitude potential Φ for the wave field by superposing two solutions : (i) known incident wave solution

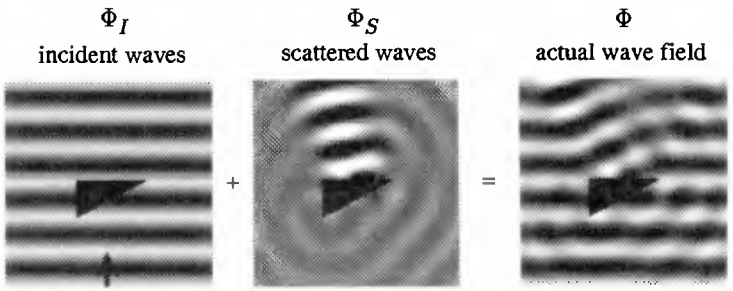

Figure 4 Collocation Method of Matched Eigenfunction Expansions

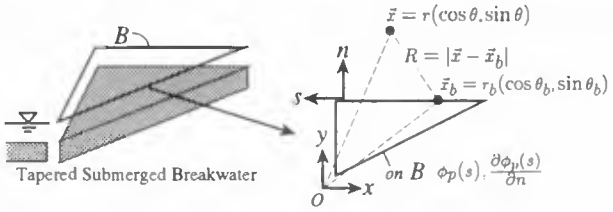

Figure 5 Definition of the symbols and integral path

Φ_I and (ii) unknown scattered wave solution Φ_S which is determined so that the whole solution ($\Phi = \Phi_I + \Phi_S$) satisfies the boundary conditions on the submerged body and Sommerfeld's radiation condition at far field (see Fig. 4).

The scattered wave solution Φ_S is expressed in terms of Green's law :

$$\Phi_S(r,\theta) = \oint_B \{\phi_B(s)\frac{\partial}{\partial n} - \frac{\partial\phi_B(s)}{\partial n}\}G(R,\theta)ds. \tag{1}$$

Here, ϕ_B and $\frac{\partial\phi_B(s)}{\partial n}$ are the potential of the scattered waves and its derivatives on the path B above the breakwater as indicated in Fig. 5, and G is the Green function. Further definitions of the symbols are depicted in the same figure.

The scattered wave solution ϕ_B consists of evanescent wave mode ϕ_E and progressive wave mode ϕ_P. The former (ϕ_E) is apparent only in the close vicinity of the structure and the latter (ϕ_P) is the wave which travels to the infinity by decaying its amplitude. Neglecting the evanescent wave, following equation for the scattered wave solution is obtained which is valid except in the vicinity of the structure :

$$\Phi_S(r,\theta) = \frac{i}{4}\oint_B \{\phi_P(s)\frac{\partial}{\partial n} - \frac{\partial\phi_P(s)}{\partial n}\}H_0^{(1)}(kR)ds \tag{2}$$

where $H_0^{(1)}$ is the Hankel function of the first kind of the 0th order and k is the wave number of the incident wave.

A further approximation is adapted to Eq.(2) to split it into radial part r and directional part θ. Following relationships of R for $r \gg r_b$ and Hankel function

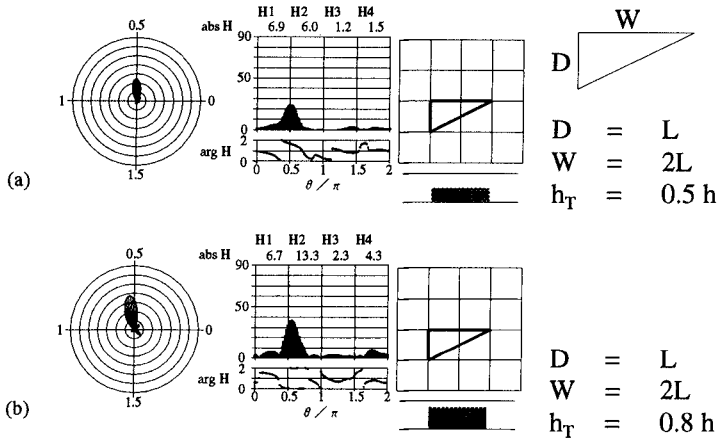

Figure 6 Distribution of Kochin function $H(\theta)$. L = incident wave length ($kh = 1.18$).

with large argument are substituted :

$$R = |\vec{x} - \vec{x_b}| \approx r - r_b \cos(\theta - \theta_b) \tag{3}$$

$$H_0^{(1)}(z) \approx \sqrt{\frac{2}{\pi z}} e^{(z-\pi/4)} \tag{4}$$

$$\frac{dH_0^{(1)}(z)}{dz} = -H_1^{(1)}(z) \approx -\sqrt{\frac{2}{\pi z}} e^{(z-3\pi/4)}. \tag{5}$$

The result of the substitution is

$$\Phi_S(r,\theta) \approx -\frac{i}{4}\sqrt{\frac{2}{\pi kr}} e^{i(kr-\pi/4)} \times \oint_B \{ik\cos(\theta - \theta_n(s))\phi_P(s) + \frac{\partial \phi_P(s)}{\partial n}\} ds \tag{6}$$

where θ_n the angle of the integral path s to the y axis.

The scattered wave solution $\Phi_S(r,\theta)$ is now separated into radial part which expresses the decay of the scattered waves travelling to the infinity, and directional part which stands for the complex amplitude of the scattered waves. The directional part is termed as *Kochin function* $H(\theta)$ (Mei, 1983).

The wave angle modification performance is estimated by comparing the characteristics of the Kochin function distribution of different TSBs. The idea is to evaluate the directional amplitude of scattered waves from Kochin function and use it as a measure of the performance. Figure 6 shows the distributions of Kochin function for TSBs with the same plane form, but of different heights. The directional distribution of $H(\theta)$ is displayed in different expressions in the figure : left diagram displays magnitude of $H(\theta)$ as a radar chart and center diagram displays magnitude and phase of $H(\theta)$. Since the incident wave travels into $\theta = 0.5\pi$, scattered waves must have wave components which travel into

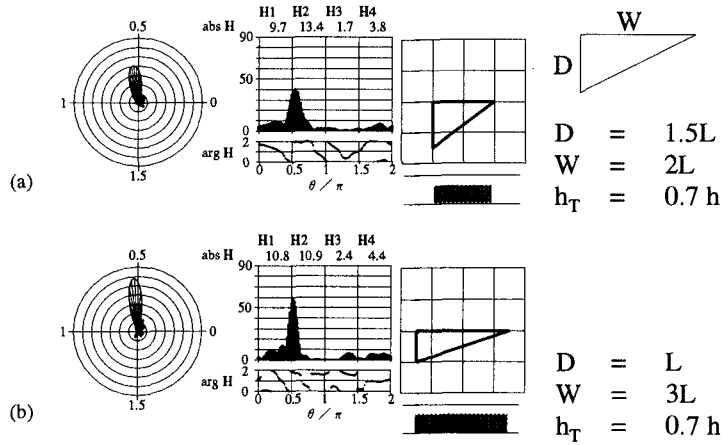

Figure 7 Distribution of Kochin function $H(\theta)$. L = incident wave length ($kh = 1.18$).

$0.5\pi < \theta < \pi$ if the wave angle modification is achieved properly. The comparison of the Kochin function distributions suggests that the TSB with larger height h_T is effective in wave angle modification.

Figure 7 shows the distributions of Kochin function for TSBs with the same height, but of different plane forms. It is hard to rate the efficiency of the two breakwaters from simple comparison of the Kochin function distributions. In this case, the integral of $H(\theta)$ in $0.5\pi < \theta < \pi$ (H_2) was estimated and used as a measure of the wave angle modification effect. The value of the integrals of different ranges is depicted in the top of the center diagram (H_1, H_2, H_3, H_4). The TSB with larger plane depth D is judged superior in wave angle modification, since it possesses a larger value.

A large number of tests for TSBs with different shapes were conducted to seek optimum configuration. It was found that heightening the height h_T and broadening the plane depth D of the breakwater enhance the effect of wave angle modification in general. It was also found that the plane depth D and the plane width W must be at least as large as incident wave length L, which means that the breakwater needs to a large structure to work well.

APPLICATION TO BED PROFILE MODIFICATION

Preliminary experiments on movable bed were conducted to test out the applicability of the TSB in topography modification. The experimental setup is shown in Fig. 8. The experiment is designed to observe the effect of wave angle modification in the offshore region on bottom topography variation and does not imply any realistic situation. The experiment started from a 1:10 slope beach made from fine glass beads with 0.08 μm mean diameter and 2.6 specific gravity.

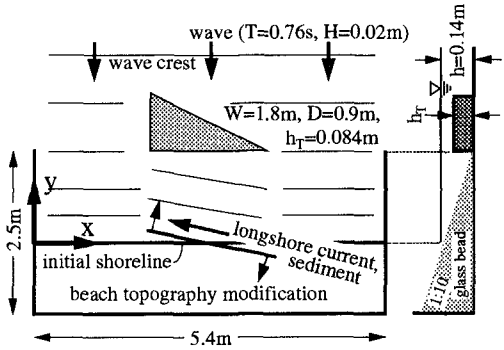

Figure 8 Experimental setup of the movable bed experiment

Regular waves with 0.76s period and $0.02m$ wave height were acted for 2 hours without installing the TSB to excite the initial off–onshore sediment movement. Then the TSB was installed in front of the slope and the experiment was proceeded further for 8 hours. Bed elevations were measured for several times during the experiment.

Figure 9(a) and (b) show the depth contour lines of the bed form at $t = 2hrs.$ and $t = 10hrs.$ for the run with single TSB. No wave breaking above the breakwater was observed. In the region of $1.7 < x < 2.8m$, the shoreline and the depth contour lines in front of it inclined remarkably at $t = 10hrs.$ which were almost straight and parallel at $t = 2hrs.$ This region was affected by the waves whose propagation angle was modified by the TSB. The distribution of total longshore sediment rate (Fig. 9(c)) estimated from the results of bed profile measurements shows that the sediment was transported unidirectional as a whole.

The wave angle modification accompanies wave concentration on the downwave side of the breakwater which results in the alongshore variation of the wave breaking point. Accordant with this breaking point variation, several circulations cells along the shore were observed which transported sediments alongshore.

Numerical computations of the wave and current field were conducted to give insight of the sediment transport. The wave field was computed with parabolic mild slope equation starting from the initial value given by the potential solution described in the previous chapter. Flow field was computed with the conventional ADI method inputting the radiation stress derived from the wave field computation. Bed profile data measured in the experiment was entered for wave and current computations.

Figure 10(a) and (b) show the computed wave height distribution and flow field at $t = 2hrs.$ The effect of wave angle modification concentrates the waves. This is shown in the figure of wave height distribution as strips of contour lines of high and low wave region. Since the high waves break at an earlier stage, the distribution of the breaking points varies alongshore. Accordant with this variation, the distribution of radiation stresses becomes complicated, and several

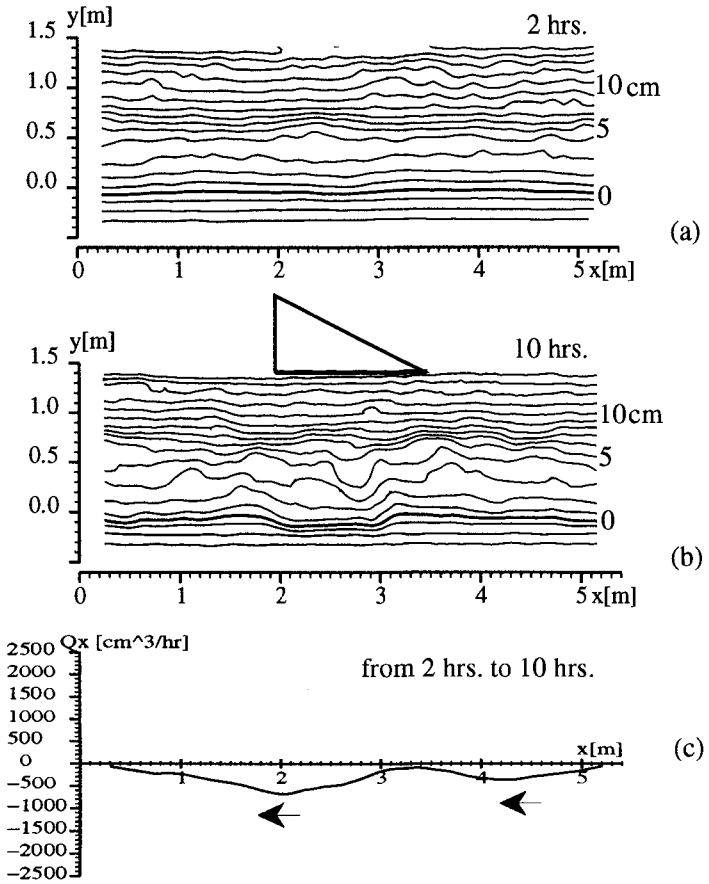

Figure 9 Resultant bed form and total longshore sediment rate, (a) $t = 2hrs.$, (b) $t = 10hrs.$, (c) Total longshore sediment rate (from $t = 2hrs.$ to $t = 10hrs.$). $W = 1.5m$, $D = 0.75m$, $h_T = 0.084m$.

circulation cells including two major counter–rotating cells are reproduced in the flow computation. Their number, position and scale agreed fairly with the experiment. It is supposed that the sediment is mainly transported by the current system. Bottom material is eroded where high waves attack. The current system then transports it as suspended sediment and deposits it finally where wave motion becomes calm.

Figure 11 shows the resultant bed form in case of two TSBs were installed in sequence. With this arrangement, it is expect that the effect of the wave angle modification extends to a wider range. The bed form at $t = 10hrs.$ shows that

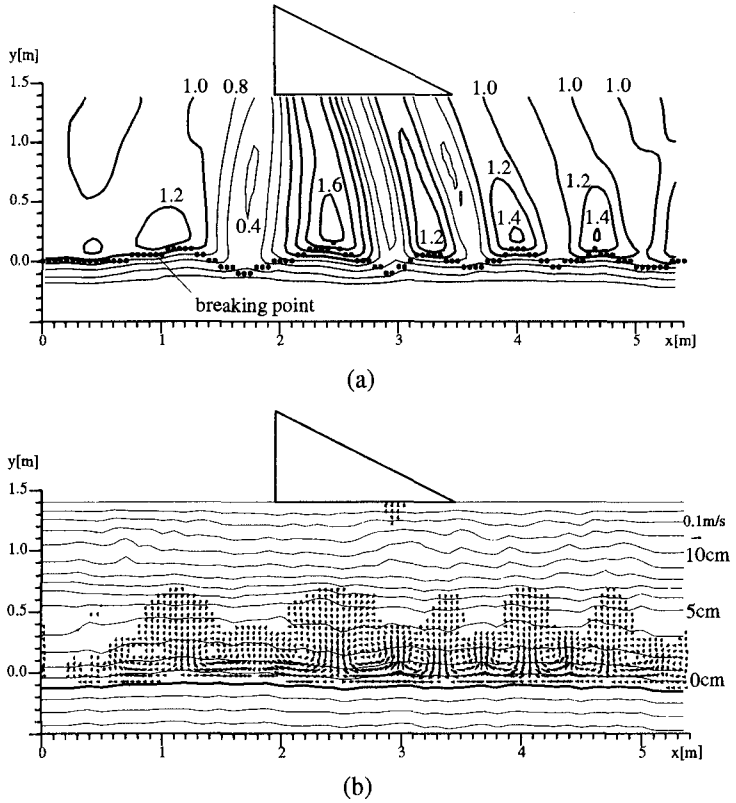

Figure 10 Computational result of wave and current system at $t = 2hrs.$, (a) Normalized wave height distribution and breaking points, (b) Current field and bed form. $W = 1.5m$, $D = 0.75m$, $h_T = 0.084m$.

each breakwater affected the sediment process individually. The distribution of total longshore sediment rate (not listed) indicates that the sediment is transported generally in the aimed direction in a wide range. It is, however, hard to conclude that the attempt is a full success. The shoreline, or depth contour lines become highly irregular and the beauty of the coast with gentle-curved or straight shoreline is lost. Further studies on this point, how to obtain a smoother shore line, are required.

CONCLUSIONS

A new type of submerged breakwater (Tapered submerged breakwater) which modifies the wave propagation angle is proposed. Its ability and performance were demonstrated and assessed analytically. TSBs with different shapes were

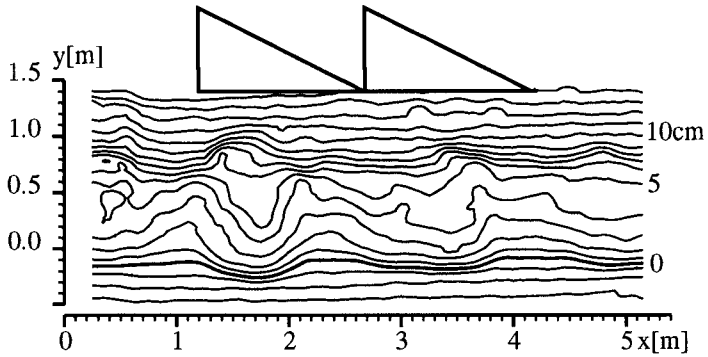

Figure 11 Resultant bed form at $t = 10hrs.$ for two TSBs run. $W = 1.5m$, $D = 0.75m$, $h_T = 0.084m$.

tested and it was found that broadening of the plane depth D and heightening the breakwater height h_T enhances the wave angle modification performance. It was also found that D and the plane width W of the TSB must be at least as large as incident wave length L to be effective. This means that the TSB needs to be a large structure to work well.

Preliminary movable bed experiments were conducted. The TSB was installed in front of the beach to modify the wave propagation angle in the offshore zone. The alongshore wave height distribution varied in the nearshore zone due to the effect of wave angle modification. Several flow circulations appeared subsequently which transported longshore sediment. The total longshore sediment rate indicates that the sediment moved unidirectional as a whole. The resultant bottom configuration, however, was highly irregular, even when two TSBs were installed in sequence. Further studies are required on this point to refine the conception acceptable.

ACKNOWLEDGMENT

Authors are indebted to Hiroshi Yamaguchi, graduate student of Kyushu University, for his collaboration in movable bed experiment.

REFERENCES

Mei, C.C (1983) : The applied dynamics of ocean surface waves, World Scientific.

Yoshida, A., Murakami K. and Ono M. (1992) : Collocation Method of Matched Eigenfunction Expansions, Proc. Japanese Conf. on Coastal Eng., JSCE, Vol.39, pp. 756 - 760 (in Japanese).

CHAPTER 156

MULTIDIRECTIONAL WAVE LOADS ON VERTICAL BREAKWATERS

Claudio Franco[1] , Jentsie W. Van der Meer[2] , Leopoldo Franco[3]

Abstract

An extensive 3-D model test program has been performed to study the effects of wave obliquity and multidirectionality on the hydraulic response of vertical (caisson) breakwaters. In this paper the results of the wave forces and pressures are shown. The measurements are compared with the Goda's formula with some divergences. The tests show that multidirectional wave loads do not reduce with increasing obliquity of the mean direction, whereas a reduction occurs for oblique long-crested waves. Three-dimensional effects on the uplift forces are better described by Goda formulations and smaller scatter is observed when comparing with measurements. The analysis of the longitudinal distribution of the horizontal pressures confirmed that the global wave load decays with increasing multidirectionality and obliquity, with clear advantages for the design of long monolithic breakwaters.

Introduction

The design of coastal structures has been typically based on formulae developed for head-on long crested waves. After the development of 3D basins in hydraulics laboratories, the effect of wave three-dimensionality on structure loading has been considered mainly for the design of offshore platforms. More recently 3-D waves were found to have influence also on the long period wave components associated to the short period waves which induce harbour oscillations (Bowers, 1987) or on the stability of rubble mound breakwaters (Galland, 1994). Very little attention has been addressed so far to the influence of wave multidirectionality on the response of vertical face structures in intermediate or shallow water .

---

[1] Ph.D. Student, DIIAR, Politecnico di Milano, P.Leonardo da Vinci 32, 20133 Milano, Italy
[2] Dr., Delft Hydraulics, p.o.box 177, 2600 MH Delft (NL) e-mail: jentsie.vdmeer @wl.delft.nl
[3] Prof. Eng., Dept.Civil Eng., 3rd University of Rome, via C.Segre 60, 00146 Rome, Italy, e-mail: leofranc@fenice.dsic.uniroma3.it

A 3-D model investigation has been carried out at Delft Hydraulics, within a joint European research project, in order to assess the effects of the obliquity and "multidirectionality" of wave attack on the hydraulic performance of caisson breakwaters. Tests have been performed with attack angles up to 60° to the normal and directional spreadings up to 30° on different structure geometries such as caissons with vertical plain wall, with perforated front wall, with an additional curved parapet and with a high impermeable slope and berm, measuring wave forces, horizontal and uplift pressures, reflection coefficients and overtopping.

Only the results of the analysis on horizontal and uplift forces on the plain wall vertical caisson are here presented in order to provide useful guidance for the design of caisson breakwaters. Comparisons are made with the more abundant results obtained by Goda (1985) on the simple vertical face structure under long-crested wave attacks.

Model setup and test conditions

The hydraulic model tests were carried out in the 26.4 m wide and 23 m long multidirectional-wave "Vinjè basin" at DH - De Voorst during summer 1994. The structure (Fig.1 and 2), consisting of 13 caissons, each 0.9 m wide, with curved roundheads at the two ends, was placed on a flat concrete bottom, and linked to the floor through a permeable two layer rock basement.

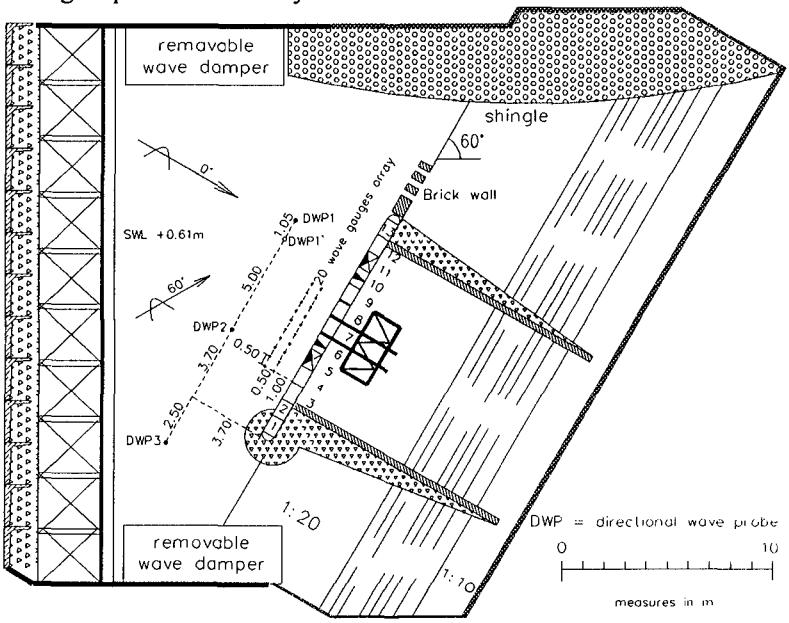

Figure 1.: Plan view of the basin and model layout

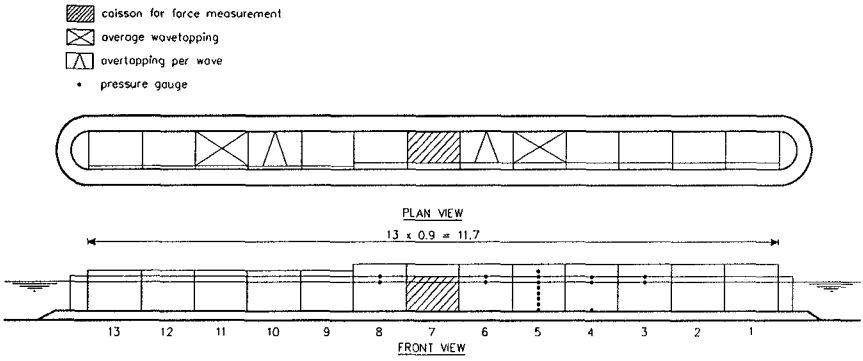

Figure 2 Plan and front view of the model caisson breakwater with location of measuring devices

Being a research model, there is no actual reference to particular prototype conditions, but a Froude scaling of 1:30 could be considered as an approximate scaling ratio for typical real structures. Crest elements were made removable in order to adjust the relative crest height (freeboard R_c/H_s = 1.18 , 1.50 and 1.63) .

The target significant wave height was kept fixed to 0.14 m throughout all tests, but the actual H_s was a little bit lower due to technical wave generation limits for the most angled wave conditions. The constant water depth in front of the caissons was 0.61 m in all tests, giving a relative water depth h/H_s=4.3. Peak periods (T_p) of standard (γ=3.3) JONSWAP spectra were 1.5 s and 2.12 s to give theoretical peak wave steepnesses $s_{op}=2\pi H_{os}/gT_p^2$ of 0.04 and 0.02 respectively. The minimum number of waves per test was 1000. Mean wave attack angles β varied with 10°steps from 0° (orthogonal to the structure axis) to the most oblique 60°. Energy dispersion around the mean direction was Gaussian with target standard deviations σ set equal to 0°, 15° and 30° (the latter two were actually 22° and 28°).

Wave conditions in front of the model have been analysed through a set of 20 gauges placed in two rows at 1.0 m distance offshore of the structure. The methods of analysis used to separate incident and reflected wave energy are the Maximum Likelihood and the Bayesian approach as explained by Frigaard et al.(1994).

A total of 84 tests with non-breaking wave conditions were performed. Of course wave breaking actually occurred before the wall when testing the caisson configuration with the frontal slope and berm. An extensive set of tests was performed for the simplest case of a straight vertical plain wall, whereas a more limited number of tests were conducted for the alternative structure geometries.

The selection of the structural configurations was based on the similarity with typical prototype conditions and with previous 2-D model studies. The basic caisson geometry (Fig. 3) was in fact designed in close agreement with a model structure

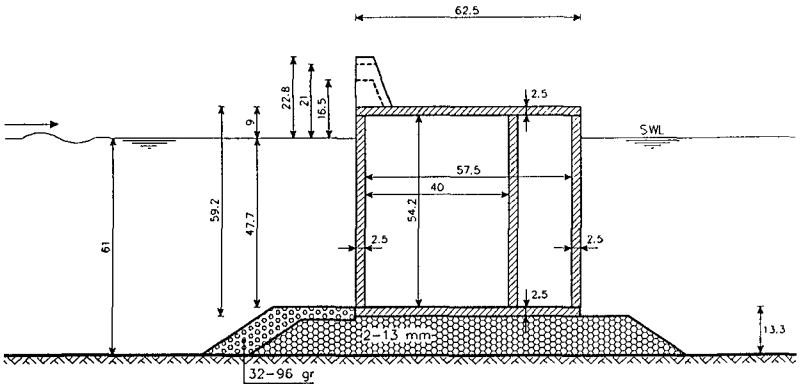

Figure 3 : Cross-section of the caisson with the simple plain vertical wall

tested in Milan for overtopping (Franco et al., 1994), while perforated walls were also designed in order to be comparable with a similar 2-D model investigation simultaneously going on at HR Wallingford, within the same MAST project. In one alternative configuration a small additional "nose" (with the same geometry tested in Milan) was placed at the top of the parapet wall, which is useful for reducing overtopping rates.

Two different types of devices have been used in the model to measure the wave-induced loads on the model structure. One central caisson (N.7 in Fig.2) was suspended above the floor of the basin by rigid metal plates attached to the inner section of the laboratory force metering frame. The inner section of the metering frame was supported by a rigidly mounted external frame section through six suspensions with strain gauges, three in the horizontal and three in the vertical planes to derive the total horizontal force F_h, the total uplift force F_u and the total overturning moment M. A clearance of approximately 2.5 mm was left around the front and sides of the measuring caisson to ensure complete freedom of movement during the force measuring tests. Two brick walls placed behind the caisson row (Fig.1) avoided wave disturbances behind the force measuring caisson.

Wave loads were also obtained by integrating data from a set of 21 pressure transducers, which were positioned on the outer vertical face (8 cells on caisson n.5), on the bottom slab (5 on caisson n.4) and along the longitudinal direction of the caisson structure (Fig.2). All pressure signals have been combined into a total horizontal force and a total uplift force by multiplying each cell output with different factors, representing the respective influence area. The uplift force was therefore achieved only from the pressure cells measurements. The output signals from both the strain gauges of the measuring frame and from the set of pressure cells were sampled at 25 Hz and filtered analogically in real-time at 12.5 Hz. This means that only the "pulsating forces" and no wave impacts would have been recorded.

Horizontal forces

The comparison between the measurements obtained with the two systems (applied on different caissons) could be performed only in the four tests with long-crested (or unidirectional) waves approaching the structure perpendicularly (β=0°). The total force over the two different longitudinal influence areas (a vertical line for the pressure transducers and a band-width of 0.9 m for the force-metering caisson) is infact influenced by wave obliquity and multi-directionality.

With the longer period waves (s_{op}=0.02) the horizontal force obtained with the pressure cells showed values 8-9% higher than those derived with the force metering frame, thus revealing a standing wave pattern along the structure length with consequent non-homogeneity of the incident wave field (Fig.4a). Other reasons that can partially explain this divergences may be the dynamic response of the free caisson (n°7) with consequent inclusion of additional inertia forces, or the different force application area which can have a small effect even under head-on wave conditions which are never perfectly two-dimensional. With the shorter waves (s_{op}=0.04) the comparison between the two measurements revealed an exact coincidence of the total force series, exception made for the highest two or three higher values (Fig.4b). In such case the pressure transducers were able to record also the faster transients that, acting only on a local scale, are not represented by the whole caisson metering system.

The general good matching of the force series confirmed the overall homogeneity of the incident wave field and thus the data reliability.

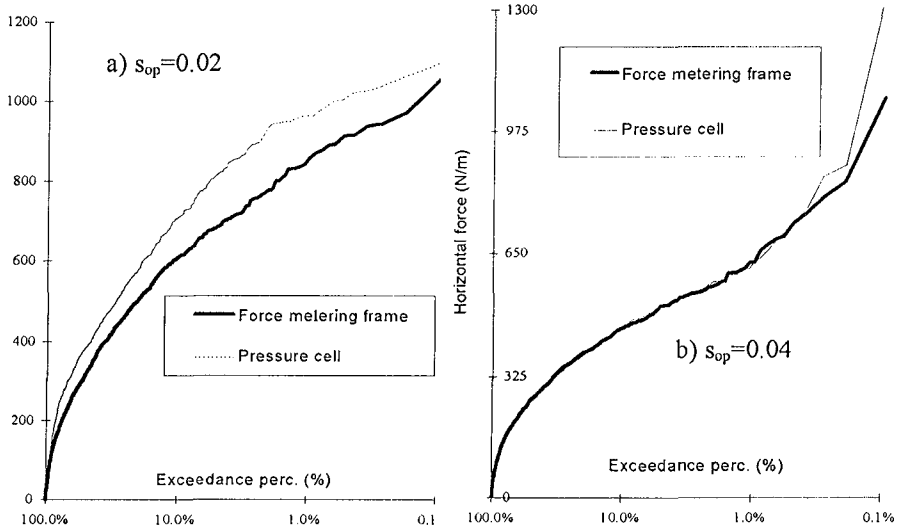

Figure 4 : Comparison between the force measurements of the pressure cells and the caisson frame outputs

The analysis has been mainly addressed to the pressure cell records, also to be consistent with the uplift force measurements which have been recorded only through the set of pressure cells. The analysis, however, demonstrated that the effects of the different wave conditions are similarly represented by both types of recordings.

The most commonly adopted prediction formula for determining the pulsating loads on vertical face structures, under long-crested attacks, is the Goda formula (1985). Design wave parameters are the maximum wave height in front of the structure H_{max} and the significant wave period T_s, which is close to the peak period T_p. Goda suggests to use as H_{max} the mean of the highest 1/250 part of the total number of waves. If Rayleigh is assumed as the probability distribution of wave heights in deep water, then $H_{max} = H_{1/250} = 1.8\ H_{si}$. Thus, the analysis has been concentrated on the $F_{h1/250}$ statistical value, which is the average of the four highest recorded forces in each of the 1000 waves-long tests. Other statistical values such as $F_{h,95\%}$, $F_{h,99\%}$, $F_{h,99.6\%}$, $F_{h,99.8\%}$, $F_{h,99.9\%}$ (the latter being the actual maximum measured force) have been used for further verification.

The little variations of the incident wave heights are taken into account when comparing forces of different tests by using the dimensionless force $F_{h,1/250}/\rho g h H_{si}$ as proposed by Goda (1985). h is the water depth in front of the structure, $\rho g = w_0$ is the specific weight of the water and H_{si} is the significant wave height measured at the structure. The graph of figure 5 clearly shows the change of this dimensionless parameter with the angle of wave attack β only for the tests with high crest. At perpendicular wave attacks, short-crestedness produces horizontal loads that are about 30% less than those acting under long-crested seas.

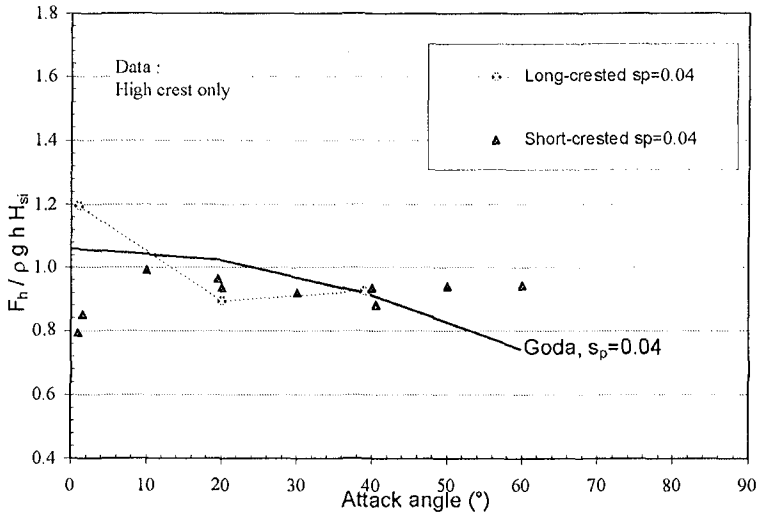

Figure 5: Horizontal forces: comparison of measurements with Goda's prediction. "h" on the y-axis is the water depth in front of the structure

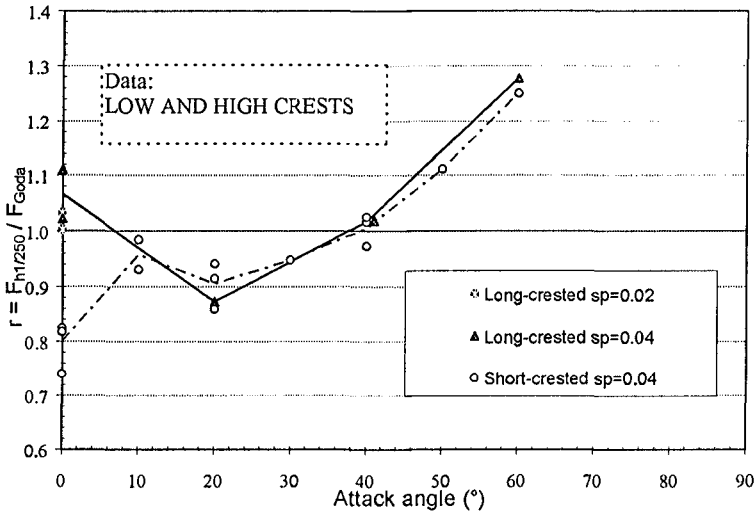

Figure 6 : Horizontal forces: reliability of the Goda formula.

This applies also for the s_p=0.02 data set, for which such comparison can be performed at β=0° only.

The most direct way to present the measured forces compared with the Goda prediction is to plot $r=F_{h,1/250} / F_{h,Goda}$ versus the angle of attack as shown in Figure 6 in which the 3-D effects are described. A general increase of r with increasing wave obliquity is clearly noted, which is due to the fact that Goda assumes a load decay with obliquity proportional to a cosine function which is not confirmed by these tests.

The average ratios between the measured $F_{h,1/250}$ and the calculated horizontal forces $F_{h,Goda}$, together with the relative standard deviations, are given in Table 1.

Table 1: r factor and shape parameter b for different wave conditions

	s_{op}	$r = F_{h,1/250} / F_{h,Goda}$		Shape parameter b	
		Mean	St.dev.	Mean	St.dev.
Long-crested waves	both	1.11	0.12	2.15	1.08
Short-crested waves (3-D)	0.04	0.96	0.14	2.00	0.47
Short-crested waves (3-D)	0.02	0.96	0.20	1.86	0.28
ALL WAVE CONDITIONS		0.99	0.14	1.95	0.67

Variation coefficients, σ/μ, amount to 10-15% . Other conclusions can be drawn from the analysis of Figures 5 and 6:

- Generally for the long-crested case, a load reduction due to the obliquity of wave attack is observed. Goda predicts this reduction fairly well (±10-12%) up to attack

angles β=40°. At β=60°however, the measured force is more than 25% higher than predicted by Goda.

- With long-crested head-on waves, Goda formula slightly (7%) underestimates the force for both wave conditions with s_{op}=0.04 and s_{op}=0.02 .
- With short-crested seas, the force shows no reduction with increasing angle of attack. Then it appears that Goda formula underestimates loads with large wave obliquities (β>40°), so it may not be suitable for representing the effect of wave obliquity in short-crested seas.
- With head-on short-crested seas, Goda prediction tends to overestimate the total horizontal force by 20% on average.

When short-crested wave conditions dominate, Goda's formulation may be modified to take into account wave multi-directionality, by including a reduction factor r_{3D} =0.8~0.85 on the total load and disregarding all the effects related due to wave obliquity β.

As far as the response of the alternative geometry with recurved parapet top ("nose"), little differences of the total F_h have been observed when comparing with the case of a simple plain wall, despite the effectiveness in reducing overtopping.

The loads acting on the tested structures have been analysed statistically. A two-parameter Weibull distribution, which is often used in extreme value problems, has been fitted to the measured horizontal forces with exceedance probability of 5%, 2%, 1%, 0.4%, 0.2% and 0.1% (the latter is the actual maximum measured force) as:

$$P(F_h) = exp\ -(F_h/a)^b \qquad (1)$$

where a is the scale parameter, b is the shape parameter and $P(F_h)$ the exceedance probability . Fig.7 shows an example of force data fitting with a two-parameter Weibull. The calculated shape parameters b are presented in Table 1 for different incident wave conditions.

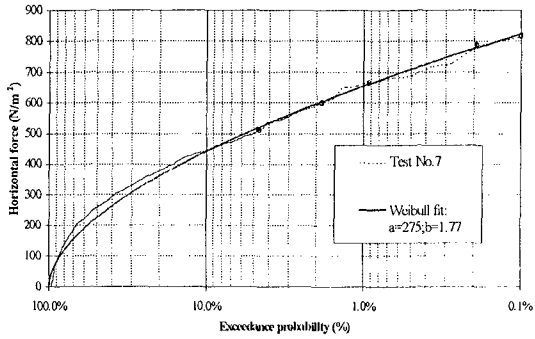

Figure 7 : Example of data fitting with the Weibull distribution.
(β=20°, σ=22°, s_{op}=0.04)

Even though variation coefficients, σ/μ, are quite large (25-50%), the mean values of "b" are found to be close to 2.0, which correspond to a Rayleigh distribution.

A design formula (Van der Meer et al., 1995) may thus be derived from equation (1) for the exceedance probability of the highest forces, based on Goda's method:

$$P(F_h) = \exp -(2.547\, F_h / (r\, F_{h,Goda}))^b \qquad (2)$$

where some "indicative" values of the shape parameters b and of the factors r are given in Table 1 for various 2-D and 3-D seastates. The coefficient 2.547 (=1/a) is obtained by substituting $P(F_{h,1/250})$=0.00152 into equation (1).

Uplift forces

The uplift force measurements are shown in Figure 8 by using the dimensionless uplift force $F_{u1/250}/\rho g B H_{si}$, as proposed by Goda (1985), where B is the bottom width of the caisson. A consistent decay of the uplift force with increasing wave obliquity for the steeper sea-state is shown, as also described by the Goda formula. A little difference (7-8%) is found at perpendicular wave attacks between the long and short-crested wave loads, but not as large as found for the horizontal force measurements. When waves are oblique the two seastates give similar results up to β=60°, where a reduction of 30-35% on the total load is observed if compared to the head-on case. The crest "nose", as expected, was found to have a marginal influence on the uplift forces. The force decay with wave obliquity matches that of the simple wall without nose for both long and short-crested wave attack.

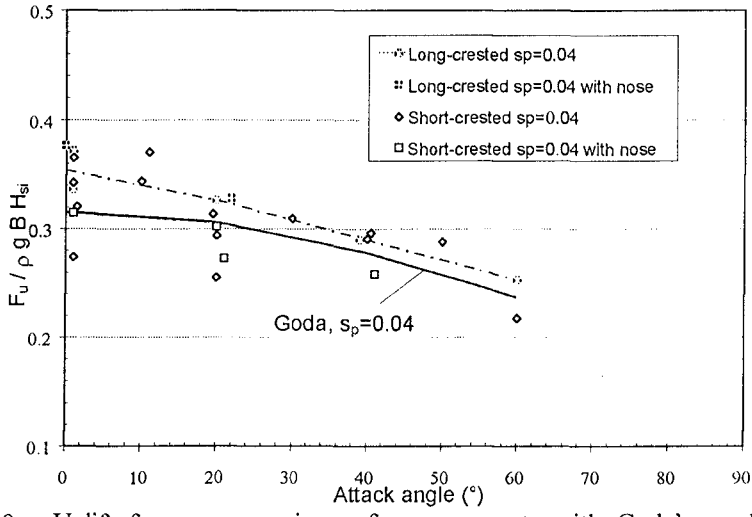

Figure 8 : Uplift forces: comparison of measurements with Goda's prediction. "B" on the y-axis is the caisson width.

The Table 2 shows the mean values and the standard deviations of $r=F_{u1/250}/F_{u,Goda}$ obtained for different wave steepnesses and multidirectionality indices. Standard deviations are generally lower than those of the horizontal forces and the mean values show a little reduction with short-crested waves. It is observed however, that wave obliquity effects on the uplift load are substantially well described by Goda's prediction. Some inaccuracy is noticed for angles up to β=20° for which the measured $F_{u1/250}$ can be on average ±15% of $F_{u,Goda}$. In the range β=30° up to β=60° the discrepancy reduces down to ±10% .

Table 2: Uplift forces: r factor and shape parameter b for different wave conditions

	s_{op}	$r = F_{u,1/250} / F_{u\,Goda}$		Shape parameter b	
		Mean	St.dev.	Mean	St.dev.
Long-crested waves	both	1.04	0.08	2.47	0.95
Short-crested waves (3-D)	0.04	1.03	0.10	2.29	0.74
Short-crested waves (3-D)	0.02	0.93	0.10	2.15	0.22
ALL WAVE CONDITIONS		0.99	0.10	2.30	0.70

Measured uplift force series have been fitted by a Weibull distribution, enabling the derivation of the scale and shape parameters for each test . Generally, the mean values of the shape parameter "b" were found to be higher than those relative to the horizontal forces, thus confirming a similar result obtained by Bruining (1994). For wave attack angles greater than 20° the shape parameter was found to be consistently higher than 2.0 (Rayleigh). For design applications the factors in Table 2 may be used as input for relation (1) with reference to F_u .

Wave pressure diagram shape

The analysis of the pressure distributions underneath and in front of the caisson revealed that few significant changes in the diagram shape occur with increasing obliquity of wave attack. When the 0.1%, 0.4%, 1%, 2%, 10% exceedance values of the total horizontal load were reached, the concurrent pressure values at the various locations have been recorded. The resulting instantaneous pressure distributions have been plotted in Fig.9 and 10 together with the calculated distribution of Goda. In the figures, attention is only focused on the diagram "shape" since comparisons in absolute terms cannot be performed, given the difference of the incident wave height in each data set and being the pressures not dimensionless.

The horizontal pressure distribution along the vertical wall, is fairly well predicted by the Goda's formula for both two and three-dimensional sea states, although the concave shape between the S.W.L and the sea bed differs from the simply linearized one by Goda . In Figure 9 the influence of wave obliquity is shown for long-crested seastate with s_p=0.04: it can be observed that the vertical distribution of the horizontal pressures is not affected by the variability of the incidence angle.

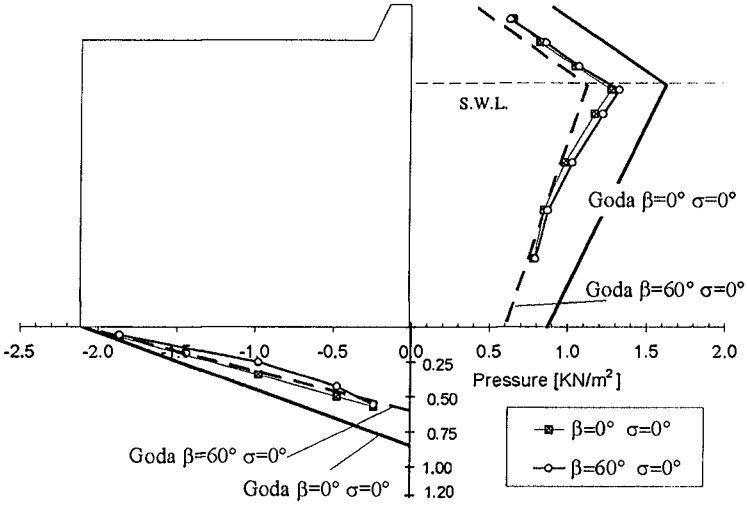

Figure 9 : Wave pressure diagram: effect of wave obliquity

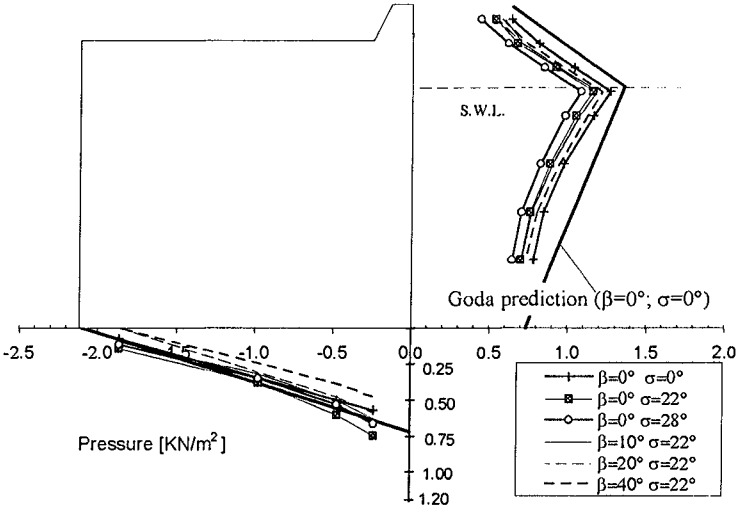

Figure 10: Wave pressure diagram: effect of wave spreading

For the uplift pressures, on the contrary, considerable changes in the diagram shape occur with increasing angle of wave attack. For large obliquity the uplift pressure distribution is not triangular (as predicted by Goda and as found in the head-on wave cases), but shows a slight concavity that shifts the centre of gravity to the seaward toe of the caisson, thus increasing the overturning moment M_u . However, the absolute value of the uplift force reduces with obliquity (not properly shown in the figure given the non-dimensionless force), so that the overall moment reduces,

even with larger arm. For most tests, the uplift distribution is fairly well in agreement with the Goda's prediction.

The effect of wave directional spreading on the uplift pressure diagram is similar to that induced by wave obliquity (Fig.10), whereas the influence of the pressure exceedance level on both the horizontal and uplift pressure distributions was found to be negligible.

Longitudinal distribution of the horizontal loads

Additional analysis has been addressed to the longitudinal distribution of the horizontal loads by coupling pressure signal time histories from adjacent caissons in various multiple combinations. Under oblique wave attack, in fact, long structures are not simultaneously subjected to the peak loads. Moreover, in short-crested seas, in which wave crests are characterised by a finite length, the correlation between the wave motion at distinct locations is lower than that achieved with long-crested waves. A global load reduction on long monolithic structures can thus be expected.

In this study, the total load decay with increasing longitudinal caisson lengths (L), as a function of peak wave length (L_p), attack angle and spreading, has been compared with the theoretically derived Battjes (1982) formula: as shown in the example of Figure 11, the agreement is reasonable for both long-crested and short-crested sea-states. Even under unidirectional head-on attack the 3-D tests showed a small load reduction, due to the finite wave width. With oblique and short-crested wave attacks the actual global load is underestimated by the theory for about $L/L_p>0.5$.

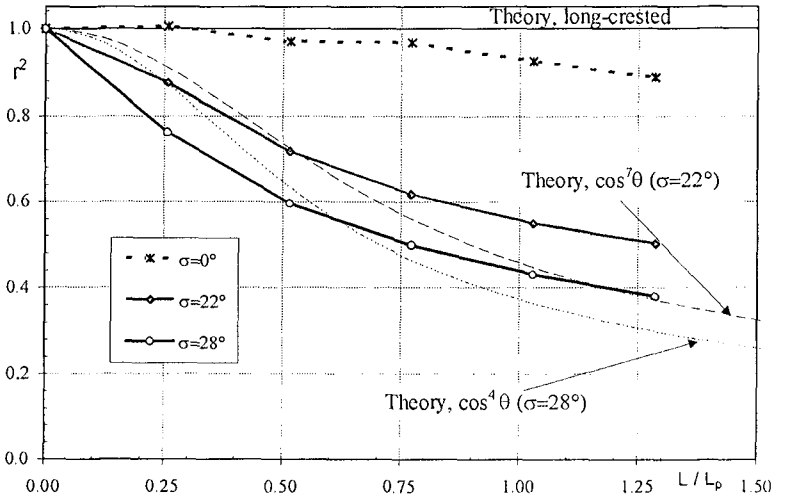

Figure 11 : Longitudinal load decay for head-on long and short-crested waves

Real 3-D waves can produce substantially reduced total loads on a vertical structure even with length as short as 0.25 L_p. Therefore the construction of new longer caissons may allow valuable savings.Various graphs from this new data set provide useful guidance for caisson breakwaters design (Franco C., 1996).

Conclusions

The results of an extensive model study on the three-dimensional wave loads on simple vertical face caissons (with and without an additional nose) has lead to the following conclusions:

- The current practice for the evaluation of design wave loads on monolithic vertical breakwaters subjected to pulsating wave loads may not be adequate in three-dimensional sea-states. The total horizontal force acting on a whole caisson should be calculated first by considering the pressure integral along a vertical section of infinitesimal width and afterwards by applying a reduction factor proportional to the caisson relative length. This reduction can be significant even for the structures commonly constructed in the practice (l=20-40 m) and it is even larger in case of impact loads, which are typically applied only on limited areas. In fact the analysis of 3-D model tests showed the coincidence of the total horizontal force measurement on a whole free caisson and the reduced averaged pressure integral of two adjacent caissons.
- The Goda formula gives a good prediction of the horizontal forces for long-crested waves approaching the breakwater at angles less than β=40° with respect to the normal. However, in short-crested sea-states it should include a correction factor of 0.8-0.85 and disregard all effects of wave obliquity.
- Three-dimensional effects on the uplift forces are better described by Goda formulations and smaller scatter is observed when comparing with measurements. However, minor changes in the shape of the pressure diagram are observed for the most oblique wave attacks.
- Even though the Weibull shape parameter b of the fitted probability distribution presents a large scatter, the highest horizontal forces can be described with Rayleigh (b=2.0), whereas slightly higher b values are found for the uplift force series.
- The global wave load on monolithic caissons with lengths as short as 0.25L_p are substantially reduced, as predicted fairly well by Battjes theory.

Additional analysis on the longitudinal decay of 3-D wave loads and on the distribution of the mean and individual wave overtopping for the various tested geometries are extensively presented in other papers (Franco et al., 1995) and in the final internal report of the research project team.

Acknowledgements

This 3-D model investigation has been financed by the UE under the Large Installation Programme (LIP) and the MAST II-MCS project and partly by Dutch Rijkswaterstaat (TAW committee). The research program was proposed and coordinated by L.Franco and J.Van der Meer; model testing was directed by J. Wouters; data analysis and interpretation was mainly conducted by C.Franco.
The authors wish to thank J.P.de Waal and P.Pasterkamp (Delft Hydraulics) and C.Restano (Politecnico Milano) for their productive cooperation and advice.
The good collaboration of the LIP-MAST partners, H.Burcharth, P.Frigaard and J.H.Petersen (Aalborg University, DK), of the other European MAST partners H. Oumeraci (LWI,D), W.Allsop (HR, UK), J.Juhl (DHI, DK), M.Canel (SOG, F) and P.Tonjes (RWS, NL) is also acknowledged .

References

BATTJES J (1982) Effects of short-crestedness on wave loads on long structures, *J Applied Ocean Research*, Vol.4 No.3 pp 165-172

BOWERS E (1987) Short-crested seas in harbour modelling, *Rep Sr141* HR Wallingford.

BRUINING J W (1994). Wave forces on vertical breakwaters. Reliability of design formula. *Msc. Thesis*, Delft Univ. of Technology. Also *D.H. report H1903*.

FRANCO C (1995) "3-D wave overtopping on caisson breakwaters", Student competition, *XXVI IAHR congress*, , London

FRANCO C., (1996), "Wave three-dimensional effects on long maritime structures" (in Italian), *IV°AIOM Congress*, Padua (I)

FRANCO C., FRANCO L., RESTANO C., PASSONI G., V.D.MEER J, (1995),"The effect of wave obliquity and short-crestedness on the overtopping rate and volume distribution on caisson breakwaters", *MAST II-MCS Final Project Proceedings*

FRANCO L., DE GERLONI M., VAN DER MEER J.W. (1994), "Wave overtopping on vertical and composite breakwaters", *Proc.of the 24th ICCE*, Kobe, ASCE, NY

FRIGAARD P PETERSEN J H (1994) Estimation of incident wave height. *MAST II-MCS LIP, 3rd Workshop*, Nov 94, De Voorst, The Netherlands.

GODA Y.(1985), Random seas and design of maritime structures .University of Tokyo Press.

VAN DER MEER, J.W. D'ANGREMOND K, JUHL J (1995) Probabilistic calculations of wave forces on vertical structures.. *DELFT HYDRAULICS publication n.487*